Time-dependent close-coupling method for electron-impact ionization of hydrogen

M. S. Pindzola
Department of Physics, Auburn University, Auburn, Alabama 36849

D. R. Schultz
Physics Division, Oak Ridge National Laboratory, Oak Ridge, Tennessee 37831-6373

(Received 12 October 1995; revised manuscript received 13 November 1995)

Electron-impact ionization of atomic hydrogen is studied by direct solution of a set of time-dependent close-coupled partial differential equations. The close-coupled equations describe the propagation of a time-evolving wave packet on a two-dimensional radial lattice. Following the collision, the wave packet is projected onto stationary states of the target to obtain probabilities for elastic and inelastic scattering processes. Ionization cross sections are calculated for various LS partial waves and compared with previous theoretical methods.

PACS number(s): 34.80.Dp

I. INTRODUCTION

The calculation of accurate electron-impact excitation and ionization cross sections for atoms remains a long-standing problem in atomic collision physics. One of the most powerful theoretical approaches is based on the solution of a set of time-independent close-coupled differential equations for the scattering wave function [1–3]. For excitation of bound states at low energies the close-coupling method can be extremely accurate. Recently, efforts have focused on the extension of the close-coupling method to excitation and ionization of bound states at intermediate energies, notably the coupled-channels optical potential method [4,5], the intermediate energy R-matrix method [6,7], the converged close-coupling method [8,9], the variational T-matrix method [10], the converged J-matrix method [11], and the eigenchannel R-matrix method [12,13]. The recent methods all seek a better representation of the continuum in the excitation process.

A second theoretical approach is based on the solution of a set of time-independent close-coupled partial differential equations for the scattering wave function [14]. The idea is to include long-range correlation effects through the use of two-dimensional radial wave functions for the excited and scattered electrons. Recently, efforts have focused on the development of numerical methods based on basis-set expansions [15–17], finite differences [18,19], and finite elements [20,21]. Despite progress on the asymptotic three-body problem [22–24], the main limitation of this second close-coupling method is matching to the boundary condition for two free electrons.

A third theoretical approach is based on the solution of time-dependent close-coupled partial differential equations for the scattering wave function. As pointed out by Bottcher [25], time evolution of a wave packet localized in space obviates the need for answers to questions about the asymptotic form of the wave function in position space or its singularities in momentum space. Recently the wave-packet approach has been applied to the calculation of two-electron atom energies [26], atomic autoionization [27], and s-wave electron scattering from hydrogen [28].

In this paper we formulate a complete LS partial wave solution of the time-dependent close-coupled partial differential equations. The method is an extension of the recent work of Wang and Callaway [18,19] to the time-dependent

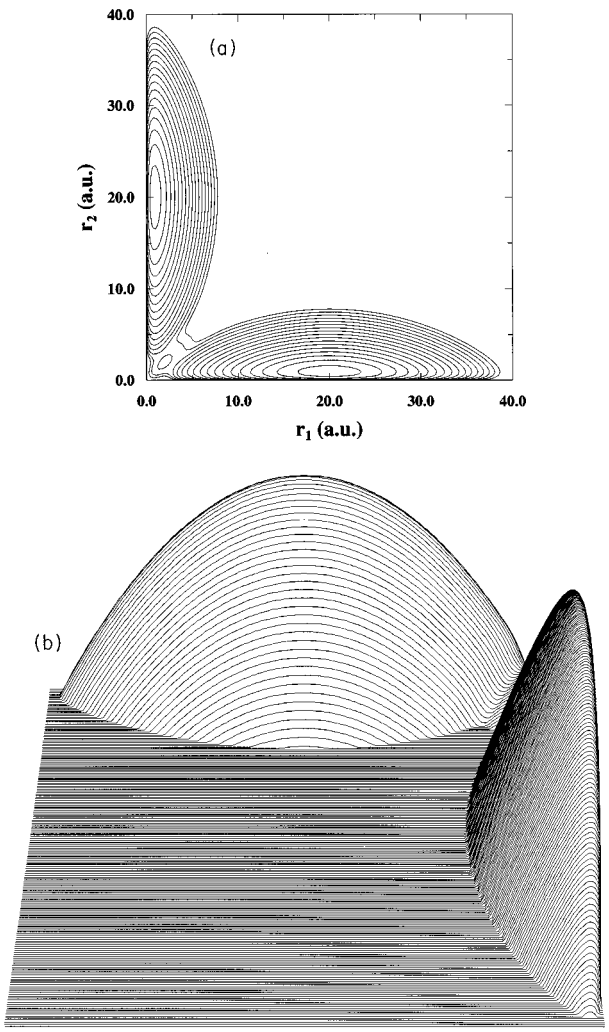

FIG. 1. $|P_{00}^{00}(r_1, r_2, t=0)|^2$ for $s=20.0$ and $w=6.0$: (a) flat contour map and (b) 3D projection.

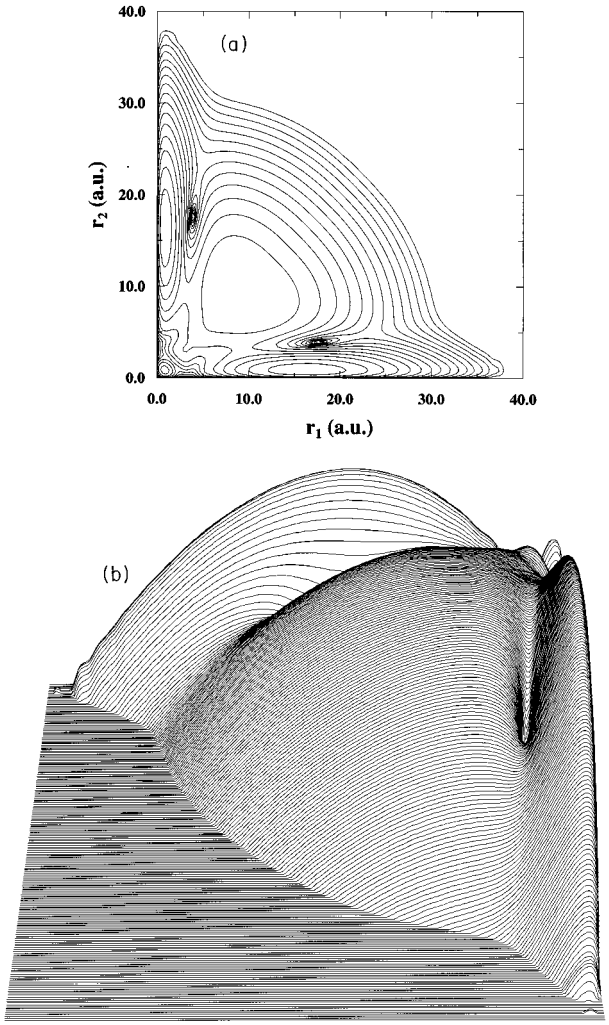

FIG. 2. $|P_{00}^{00}(r_1,r_2,t=25)|^2$ for $E=30$ eV in the Temkin-Poet model: (a) flat contour map and (b) 3D projection.

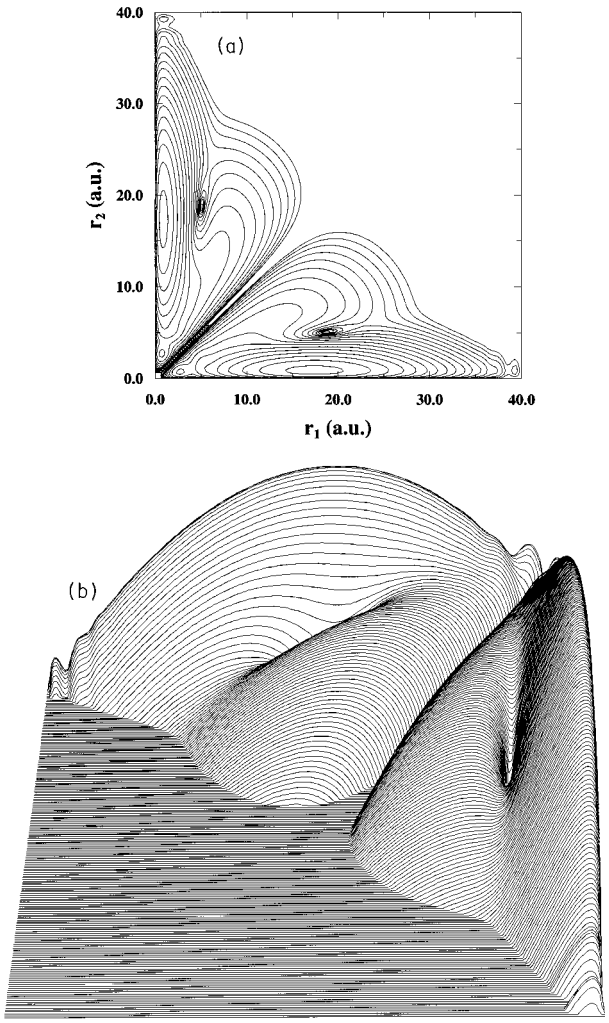

FIG. 3. $|P_{00}^{01}(r_1,r_2,t=25)|^2$ for $E=30$ eV in the Temkin-Poet model: (a) flat contour map and (b) 3D projection.

domain. We then calculate various LS partial wave cross sections for the electron-impact ionization of hydrogen. For $^{1,3}S$ scattering, restricted to s waves, we compare the cross-section results with numerous other methods. For full ^1S, ^3S, ^1P, and ^3P scattering, we compare the cross-section results with those of the converged close-coupling method [9]. Finally, we compare $^{1,3}S$ and $^{1,3}P$ partial wave results with ionization cross sections calculated in a first-order distorted-wave approximation using prior [29] and post [30] forms of the scattering potentials. It is important to understand the limitations of first-order perturbation theories, since they still remain the only viable theoretical approach for many complex atoms and molecules.

II. THEORY

For electron scattering from a one-electron target atom, the Hamiltonian (in atomic units) is given by

TABLE I. Electron-impact ionization cross sections for hydrogen in the ^1S Temkin-Poet model.

Energy (eV)	Time-dependent method Cross sections (10^{-18} cm^2)	Time-independent method [8,34] Cross sections (10^{-18} cm^2)
20.0	1.18	1.36
25.0	1.76	1.85
30.0	1.93	2.01
35.0	1.91	1.88
40.0	1.79	1.78
45.0	1.63	1.58
50.0	1.48	1.41

TABLE II. Electron-impact ionization cross sections for hydrogen in the ^3S Temkin-Poet model.

Energy (eV)	Time-dependent method Cross sections (10^{-18} cm^2)	Time-dependent method [8,34] Cross sections (10^{-18} cm^2)
20.0	0.03	0.02
25.0	0.08	0.07
30.0	0.14	0.12
35.0	0.20	0.18
40.0	0.24	0.22
45.0	0.28	0.25
50.0	0.30	0.27

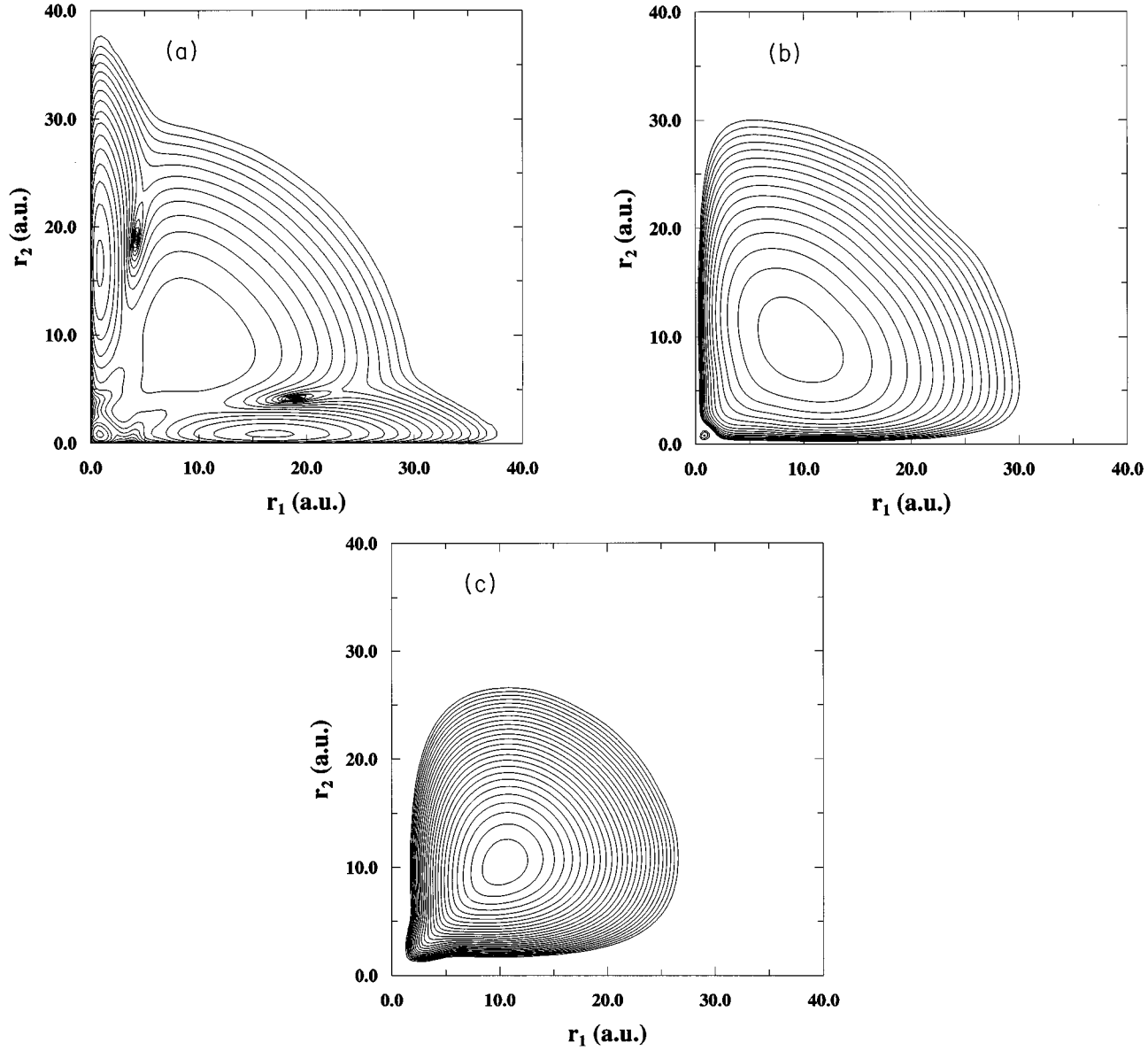

FIG. 4. $|P^{00}_{\ell_1\ell_2}(r_1,r_2,t=25)|^2$ for $E=30$ eV for a three-channel close-coupling calculation: (a) $\ell_1=\ell_2=0$, (b) $\ell_1=\ell_2=1$, and (c) $\ell_1=\ell_2=2$.

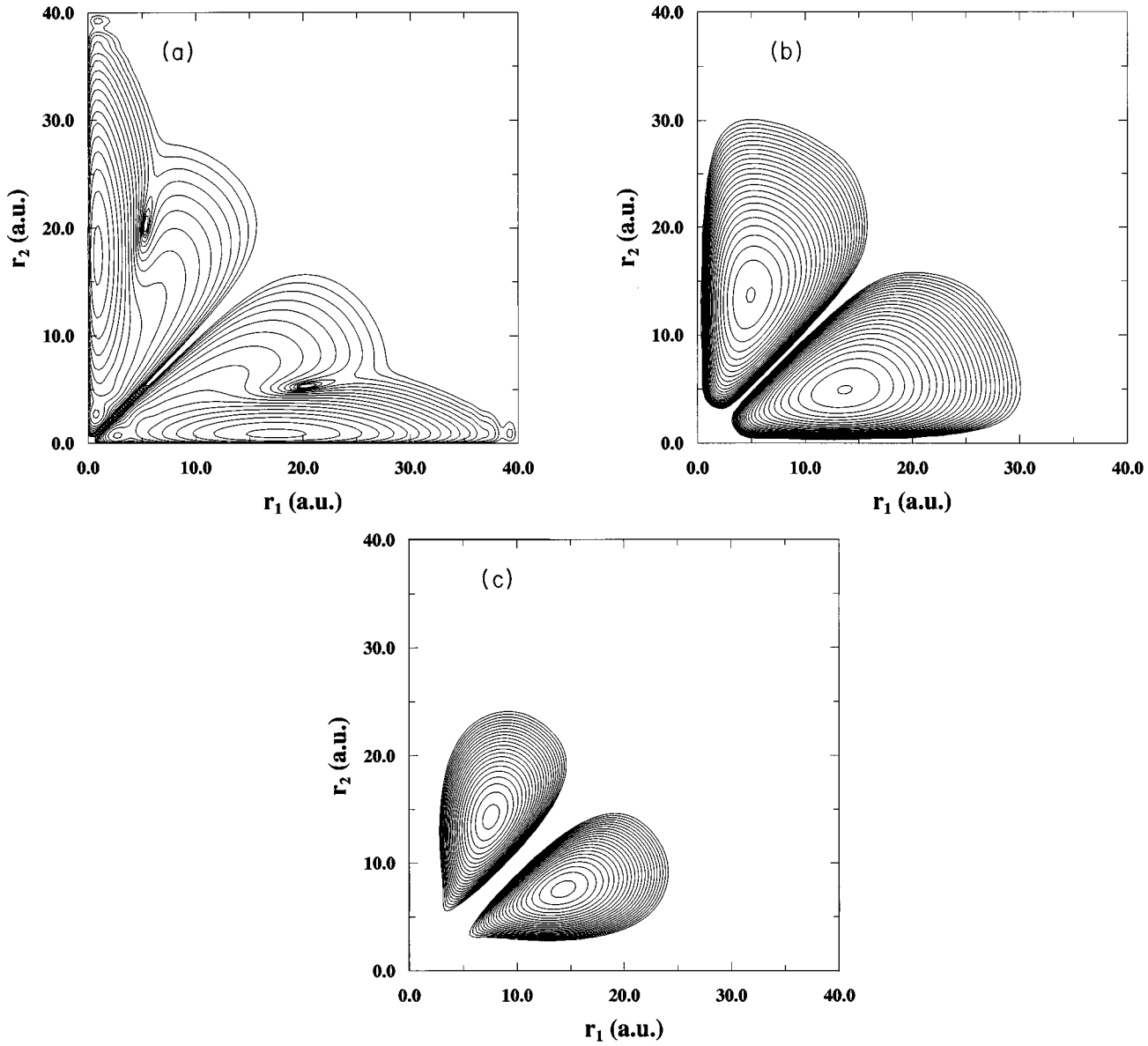

FIG. 5. $|P^{01}_{\ell_1\ell_2}(r_1,r_2,t=25)|^2$ for $E=30$ eV for a three-channel close-coupling calculation: (a) $\ell_1=\ell_2=0$, (b) $\ell_1=\ell_2=1$, and (c) $\ell_1=\ell_2=2$.

$$H=-\frac{1}{2}\nabla_1^2-\frac{1}{2}\nabla_2^2-\frac{Z}{r_1}-\frac{Z}{r_2}+\frac{1}{|\vec{r}_1-\vec{r}_2|}, \tag{1}$$

where the $\vec{r}_1$ and $\vec{r}_2$ are the coordinates of the two electrons and Z is the atomic number. The total wave function may be expanded in coupled spherical harmonics

$$\Psi^{LS}(\vec{r}_1,\vec{r}_2,t)=\sum_{\ell_1,\ell_2}\frac{P^{LS}_{\ell_1\ell_2}(r_1,r_2,t)}{r_1r_2}W^L_{\ell_1\ell_2}(\hat{r}_1,\hat{r}_2), \tag{2}$$

where

$$W^L_{\ell_1\ell_2}(\hat{r}_1,\hat{r}_2)=\sum_{m_1,m_2}C^{\ell_1\ell_2L}_{m_1m_20}Y_{\ell_1m_1}(\hat{r}_1)Y_{\ell_2m_2}(\hat{r}_2), \tag{3}$$

L and S are the total orbital and spin angular momentum of the system, $Y_{\ell m}(\hat{r})$ is a spherical harmonic, and $C^{\ell_1\ell_2\ell_3}_{m_1m_20}$ is a Clebsch-Gordan coefficient. From projection onto the time-dependent Schrodinger equation

$$\int W^{L*}_{\ell_1\ell_2}(\hat{r}_1,\hat{r}_2)\left(H-i\frac{\partial}{\partial t}\right)\Psi^{LS}(\vec{r}_1,\vec{r}_2,t)d\hat{r}_1d\hat{r}_2=0, \tag{4}$$

we obtain the following set of time-dependent close-coupled partial differential equations for each LS symmetry:

TABLE III. Convergence of the close-coupling method for $^{1,3}S$ electron ionization of hydrogen at 30 eV incident energy.

$\ell_1\ell_2$ pairs	^1S cross sections (10^{-18} cm^2)	^3S cross sections (10^{-18} cm^2)
s^2	1.93	0.14
s^2+p^2	2.82	0.31
$s^2+p^2+d^2$	2.90	0.33

$$i\frac{\partial P^{LS}_{\ell_1\ell_2}(r_1,r_2,t)}{\partial t}=T_{\ell_1\ell_2}(r_1,r_2)P^{LS}_{\ell_1\ell_2}(r_1,r_2,t)+\sum_{\ell_1',\ell_2'}V^{L}_{\ell_1\ell_2,\ell_1'\ell_2'}(r_1,r_2)\times P^{LS}_{\ell_1'\ell_2'}(r_1,r_2,t), \tag{5}$$

where

$$T_{\ell_1\ell_2}(r_1,r_2)=-\frac{1}{2}\frac{\partial^2}{\partial r_1^2}-\frac{1}{2}\frac{\partial^2}{\partial r_2^2}+\frac{\ell_1(\ell_1+1)}{2r_1^2}+\frac{\ell_2(\ell_2+1)}{2r_2^2}-\frac{Z}{r_1}-\frac{Z}{r_2} \tag{6}$$

and the coupling operator is given by [19]

$$V^{L}_{\ell_1\ell_2,\ell_1'\ell_2'}(r_1,r_2)=(-1)^{L+\ell_2+\ell_2'}\sqrt{(2\ell_1+1)(2\ell_1'+1)(2\ell_2+1)(2\ell_2'+1)}\times\sum_{\lambda}\frac{r_<^{\lambda}}{r_>^{\lambda+1}}\begin{pmatrix}\ell_1 & \lambda & \ell_1'\\ 0 & 0 & 0\end{pmatrix}\begin{pmatrix}\ell_2 & \lambda & \ell_2'\\ 0 & 0 & 0\end{pmatrix}\begin{Bmatrix}L & \ell_2' & \ell_1'\\ \lambda & \ell_1 & \ell_2\end{Bmatrix}. \tag{7}$$

We solve the time-dependent close-coupled equations using lattice techniques to obtain a discrete representation of the radial wave functions and all operators on a two-dimensional grid. When finite-difference methods are employed, local operators become diagonal matrices and derivative operators, such as the kinetic energy, have lattice representations in terms of banded matrices. For simplicity, all calculations discussed here implement uniform mesh spacing.

Stationary states of the one-electron target atom are constructed by diagonalization of the matrix representation of the radial single-particle Hamiltonian

$$h=-\frac{1}{2}\frac{\partial^2}{\partial r^2}+\frac{\ell(\ell+1)}{2r^2}-\frac{Z}{r}. \tag{8}$$

For 200 uniform grid points over the range 0–40, there are generally bound radial orbitals up to $n=5$ for each orbital angular momentum ℓ. The remaining orbitals have positive energy and represent the continuum. Only the low-n orbitals are spectroscopic, i.e., compare well in energy and form with the known hydrogenic solutions.

The total wave function at time $t=0$ is constructed as the antisymmetrized product of an incoming radial wave packet for one electron and the lowest-energy bound stationary state of the other electron [25]. For $L=0$, then

$$P^{0S}_{00}(r_1,r_2,t=0)=\sqrt{\frac{1}{2}}[g_{ks}(r_1)P_{1s}(r_2)+(-1)^S P_{1s}(r_1)g_{ks}(r_2)], \tag{9}$$

TABLE IV. Electron-impact ionization cross sections for ^1S scattering from hydrogen.

Energy (eV)	Time-dependent method Cross sections (10^{-18} cm^2)	Time-independent method [9,35] Cross sections (10^{-18} cm^2)
20.0	2.17	2.72
25.0	2.89	3.00
30.0	2.90	2.91
35.0	2.79	2.73
40.0	2.57	2.53
45.0	2.29	2.23
50.0	2.08	1.94

TABLE V. Electron-impact ionization cross sections for ^3S scattering from hydrogen.

Energy (eV)	Time-dependent method Cross sections (10^{-18} cm^2)	Time-independent method [9,35] Cross sections (10^{-18} cm^2)
20.0	0.09	0.06
25.0	0.22	0.22
30.0	0.33	0.33
35.0	0.44	0.45
40.0	0.53	0.50
45.0	0.57	0.53
50.0	0.61	0.55

and for $L \neq 0$ and $\ell = L$,

$$P^{LS}_{\ell 0}(r_1, r_2, t=0) = \sqrt{\tfrac{1}{2}}\, g_{k\ell}(r_1) P_{1s}(r_2),$$

$$P^{LS}_{0\ell}(r_1, r_2, t=0) = (-1)^S \sqrt{\tfrac{1}{2}}\, P_{1s}(r_1) g_{k\ell}(r_2), \quad (10)$$

where

$$g_{k\ell}(r) = \frac{1}{(w^2\pi)^{1/4}} e^{-(r-s)^2/2w^2} h^-_\ell(kr), \quad (11)$$

k is the linear momentum, s is the localization radius of the wave packet, w is the width of the wave packet, and $h^-_\ell(kr)$ is an asymptotic Hankel function, i.e., $h^-_\ell(kr) = e^{-ikr} e^{i\pi\ell/2}$.

For a given LS symmetry, the time evolution of the coupled equations is given by

$$\begin{pmatrix} \mathbf{P}_1(t+\Delta t) \\ \mathbf{P}_2(t+\Delta t) \\ \vdots \\ \mathbf{P}_N(t+\Delta t) \end{pmatrix} = \exp\left\{ -i \begin{pmatrix} \mathbf{T}_{11}+\mathbf{V}_{11} & \mathbf{V}_{12} & \cdots & \mathbf{V}_{1N} \\ \mathbf{V}_{21} & \mathbf{T}_{22}+\mathbf{V}_{22} & \cdots & \vdots \\ \vdots & \vdots & \ddots & \vdots \\ \mathbf{V}_{N1} & \cdots & \cdots & \mathbf{T}_{NN}+\mathbf{V}_{NN} \end{pmatrix} \Delta t \right\} \begin{pmatrix} \mathbf{P}_1(t) \\ \mathbf{P}_2(t) \\ \vdots \\ \mathbf{P}_N(t) \end{pmatrix}, \quad (12)$$

where Δt is a small time step and N is the number of $\ell_1\ell_2$ pairs. The dimension of $\mathbf{P}_i$ is equal to the number of points on a two-dimensional lattice N and the dimension of the matrices $\mathbf{T}_{ii}$ and $\mathbf{V}_{ii}$ is equal to $N \times N$. Typically

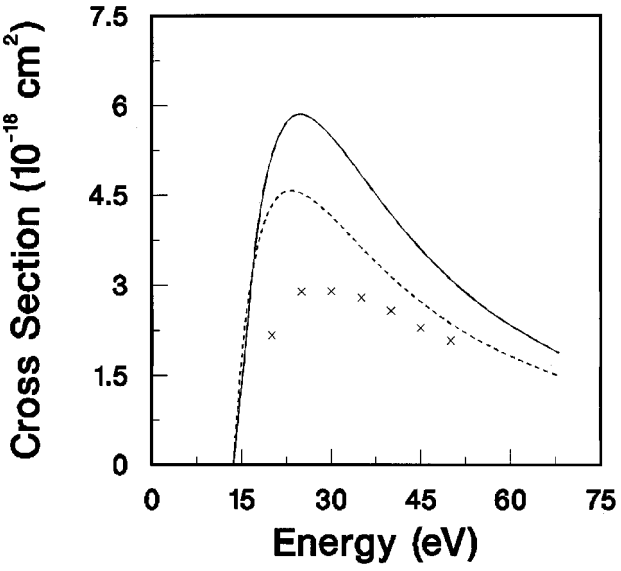

FIG. 6. Electron-impact ionization of hydrogen in the ^1S symmetry. Solid curve, distorted-wave method, prior form; dashed curve, distorted-wave method, post form; cross marks: time-dependent close-coupling method.

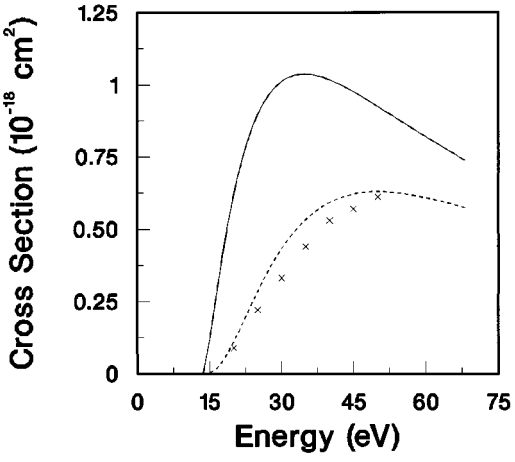

FIG. 7. Electron-impact ionization of hydrogen in the ^3S symmetry. Solid curve: distorted-wave method, prior form; dashed curve: distorted-wave method, post form; cross marks, time-dependent close-coupling method.

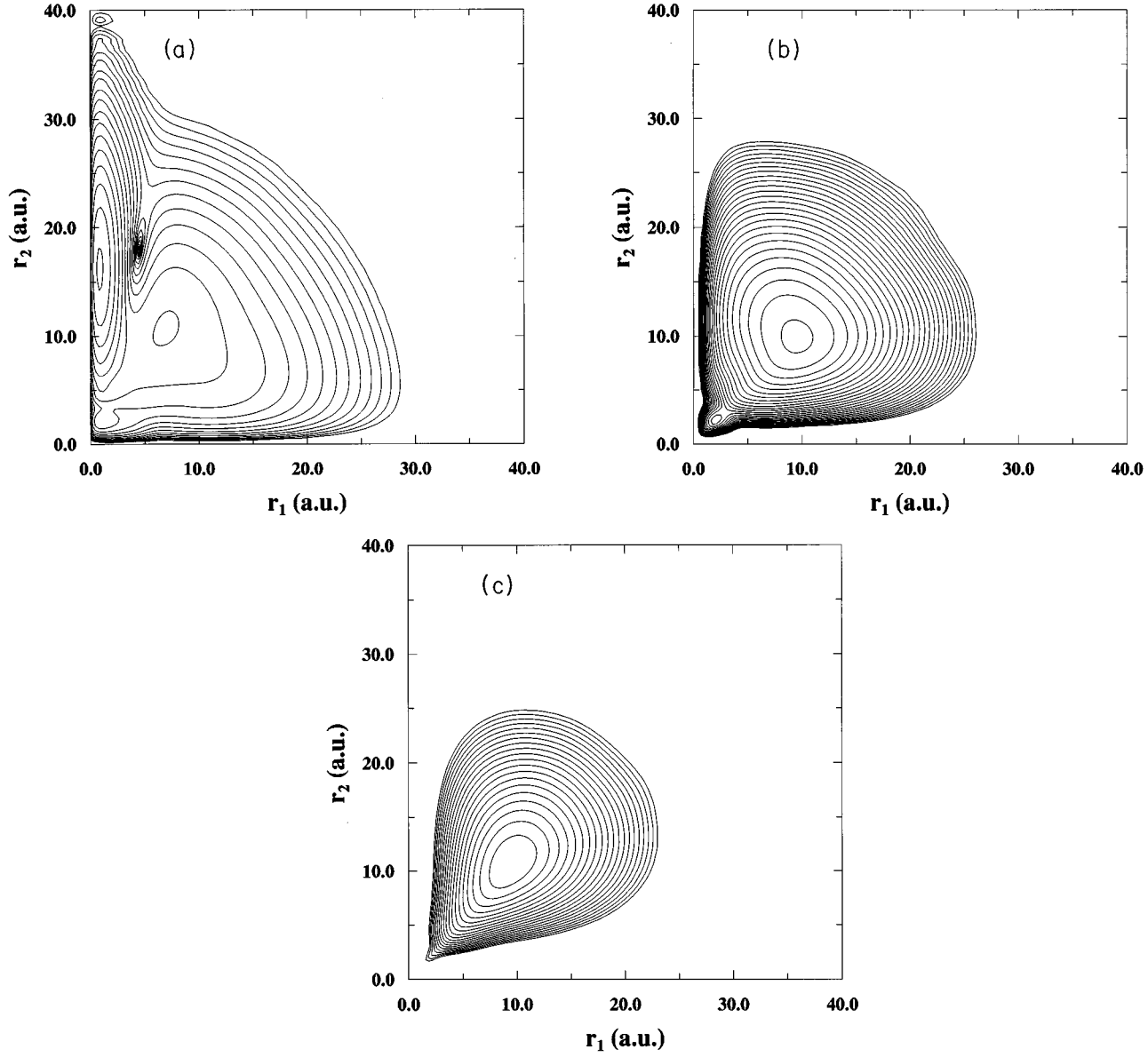

FIG. 8. $|P^{10}_{\ell_1\ell_2}(r_1,r_2,t=25)|^2$ for $E=30$ eV for a six-channel close-coupling calculation: (a) $\ell_1=0,\ell_2=1$; (b) $\ell_1=1,\ell_2=2$; and (c) $\ell_1=2,\ell_2=3$.

$\bar{N}=40\,000$. We approximate the exponential operator by a Taylor-series expansion, generally retaining 10–20 terms depending on the time step. The Taylor series is not explicitly unitary, but in practice, the norm of the wave function can be conserved to high precision.

The spin-averaged electron-impact ionization cross section is given by [28]

$$\sigma_{\rm ion}=\frac{\pi}{4k^2}\sum_{L,S}(2L+1)(2S+1)\wp^{LS}_{\rm ion}, \tag{13}$$

where

$$\wp^{LS}_{\rm ion}=1-\sum_{n,\ell,m}\wp^{LS}_{n,\ell,m}-\sum_{n,\ell,m}\sum_{n',\ell',m'}\times|\langle\Psi^{LS}(\vec{r}_1,\vec{r}_2,t)|\phi_{n'\ell'm'}(\vec{r}_1)\phi_{n\ell m}(\vec{r}_2)\rangle|^2. \tag{14}$$

In the above equations, $\wp^{LS}_{\rm ion}$ is the probability for ionization and $\wp^{LS}_{n\ell m}$ is the probability of finding only one electron in a bound state $\phi_{n\ell m}(\vec{r})$ and the other electron in the continuum.

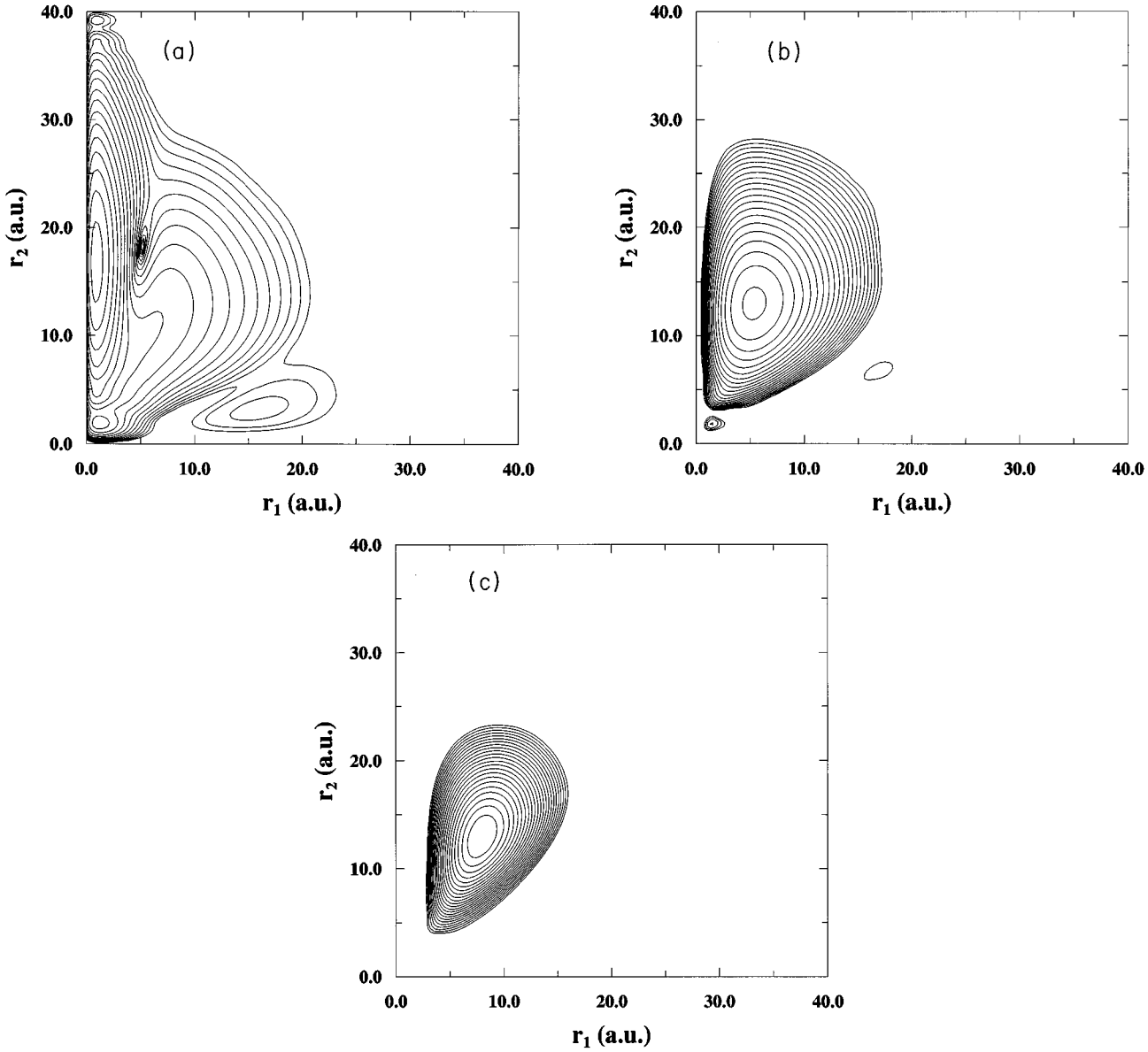

FIG. 9. $|P^{11}_{\ell_1\ell_2}(r_1,r_2,t=25)|^2$ for $E=30$ eV for a six-channel close-coupling calculation: (a) $\ell_1=0,\ell_2=1$; (b) $\ell_1=1,\ell_2=2$; and (c) $\ell_1=2,\ell_2=3$.

The third term on the right-hand side of Eq. (14) is the probability to find both electrons in bound states. The bound-state probabilities are given by

$$\wp^{LS}_{n\ell m}=\int d\vec{r}_1|\langle\Psi^{LS}(\vec{r}_1,\vec{r}_2,t)|\phi_{n\ell m}(\vec{r}_2)\rangle|^2 - \sum_{n',\ell',m'}|\langle\Psi^{LS}(\vec{r}_1,\vec{r}_2,t)|\phi_{n'\ell'm'}(\vec{r}_1)\phi_{n\ell m}(\vec{r}_2)\rangle|^2 + \int d\vec{r}_2|\langle\Psi^{LS}(\vec{r}_1,\vec{r}_2,t)|\phi_{n\ell m}(\vec{r}_1)\rangle|^2 - \sum_{n',\ell',m'}|\langle\Psi^{LS}(\vec{r}_1,\vec{r}_2,t)|\phi_{n\ell m}(\vec{r}_1)\phi_{n'\ell'm'}(\vec{r}_2)\rangle|^2. \tag{15}$$

Angular reduction of the overlap integrals found in the above equations is straightforward:

$$\sum_m\int d\vec{r}_1|\langle\Psi^{LS}(\vec{r}_1,\vec{r}_2,t)|\phi_{n\ell m}(\vec{r}_2)\rangle|^2 = \sum_{\ell_1}\delta(\ell_1\ell L)\int_0^\infty dr_1\left[\int_0^\infty dr_2 P^{LS}_{\ell_1\ell}(r_1,r_2,t)P_{n\ell}(r_2)\right]^2 \tag{16}$$

and

$$\sum_{m,m'}|\langle\Psi^{LS}(\vec{r}_1,\vec{r}_2,t)|\phi_{n'\ell'm'}(\vec{r}_1)\phi_{n\ell m}(\vec{r}_2)\rangle|^2 = \delta(\ell'\ell L)\left[\int_0^\infty dr_1\int_0^\infty dr_2 P^{LS}_{\ell'\ell}(r_1,r_2,t) \times P_{n'\ell'}(r_1)P_{n\ell}(r_2)\right]^2, \tag{17}$$

TABLE VI. Convergence of the close-coupling method for $^{1,3}P$ electron ionization of hydrogen at 30 eV incident energy.

$\ell_1\ell_2$ pairs	^1P cross sections (10^{-18} cm^2)	^3P cross sections (10^{-18} cm^2)
$sp+ps$	3.02	1.22
$sp+ps+pd+dp$	4.02	1.52
$sp+ps+pd+dp+df+fd$	4.07	1.56

where $\delta(\ell_1\ell_2\ell_3)$ indicates an algebraic triangle relation.

III. TEMKIN-POET MODEL RESULTS

If we consider only $L=0$ and restrict the sum over $\ell_1\ell_2$ pairs in Eq. (5) to just $\ell_1=\ell_2=0$, we obtain the time-dependent partial differential equation

$$i\frac{\partial P_{00}^{0S}(r_1,r_2,t)}{\partial t}=[T_{00}(r_1,r_2)+V_{00,00}^0(r_1,r_2)]P_{00}^{0S}(r_1,r_2,t), \tag{18}$$

where the operator V has the simple form

$$V_{00,00}^0(r_1,r_2)=\frac{1}{r_>}. \tag{19}$$

The time-independent version of the above equations was first proposed by Temkin [14] and subsequently solved by Poet [31–33]. Since that time most new theoretical approaches to electron-atom scattering have found their first tests on what is now called the Temkin-Poet model.

A three-point finite-difference method was employed to solve Eq. (18) on a 200×200 lattice. Each radial direction from 0–40 was spanned by a uniform mesh with spacing of 0.20. Due to the coarse grid spacing near the origin, the bound-state energy for the $1s$ state in a potential of $-1/r$ is -13.5 eV. Of course, a much larger lattice size has the effect of correcting the bound-state energy spectrum. We are looking forward, however, to solving Eq. (5) with as many as six coupled channels and a large lattice becomes computationally expensive. The Temkin-Poet model serves as a good test for determining minimum lattice sizes.

At time $t=0$ the wave packet was given a localization radius of 20.0 and a width of 6.0. The absolute value squared of the initial radial wave function of Eq. (9) is shown in Fig. 1. The two large mounds are due to the antisymmetrized product wave function. The shape of each mound is determined by the wave-packet width in one direction and the $1s$ bound-state orbital width in the other direction. As time increases the wave packet first collapses to the origin and then rebounds outwards. At time $t=25.0$ and 500 time steps, the absolute value squared of a radial wave function with $S=0$ and $E=30$ eV is shown in Fig. 2, while the radial wave-function density with $S=1$ and $E=30$ eV is shown in Fig. 3. The surviving mounds along each axis represent elastic scattering and excitation to low-lying bound excited states. The wave-packet density in the vicinity of the $r_1=r_2$ ridge represents ionization. At every 20 time steps the bound and continuum state probabilities of Eqs. (14) and (15) are computed. By the time $t=25.0$ all the probabilities have settled down to their final steady-state values and cross sections may be calculated.

Electron-impact ionization cross sections for hydrogen in the Temkin-Poet model are presented in Tables I and II for a number of incident energies. In Tables I and II the $^{1,3}S$ symmetry time-dependent results are compared with the time-independent converged close-coupling results of Bray and Stelbovics [8,34]. The ^1S and ^3S ionization cross sections presented in the tables are also in good agreement with other recent Temkin-Poet model calculations [13,15,17,28].

IV. $^{1,3}S$ PARTIAL-WAVE RESULTS

We now consider $L=0$ and begin with the close-coupled set of partial differential equations given by

$$\begin{aligned}i\frac{\partial P_{00}^{0S}(r_1,r_2,t)}{\partial t}=&[T_{00}(r_1,r_2)+V_{00,00}^0(r_1,r_2)]P_{00}^{0S}(r_1,r_2,t)\\&+V_{00,11}^0(r_1,r_2)P_{11}^{0S}(r_1,r_2,t)\\&+V_{00,22}^0(r_1,r_2)P_{22}^{0S}(r_1,r_2,t),\\ i\frac{\partial P_{11}^{0S}(r_1,r_2,t)}{\partial t}=&[T_{11}(r_1,r_2)+V_{11,11}^0(r_1,r_2)]P_{11}^{0S}(r_1,r_2,t)\\&+V_{11,00}^0(r_1,r_2)P_{00}^{0S}(r_1,r_2,t)\\&+V_{11,22}^0(r_1,r_2)P_{22}^{0S}(r_1,r_2,t),\end{aligned}$$

TABLE VII. Electron-impact ionization cross sections for ^1P scattering from hydrogen.

Energy (eV)	Time-dependent method Cross sections (10^{-18} cm^2)	Time-independent method [9,35] Cross sections (10^{-18} cm^2)
30.0	4.07	5.04
40.0	3.94	4.41
50.0	3.35	3.74

TABLE VIII. Electron-impact ionization cross sections for ^3P scattering from hydrogen.

Energy (eV)	Time-dependent method Cross sections (10^{-18} cm^2)	Time-independent method [9,35] Cross sections (10^{-18} cm^2)
30.0	1.56	1.65
40.0	1.46	1.51
50.0	1.34	1.44

$$i\frac{\partial P_{22}^{0S}(r_1,r_2,t)}{\partial t}=[T_{22}(r_1,r_2)+V_{22,22}^0(r_1,r_2)]P_{22}^{0S}(r_1,r_2,t)+V_{22,00}^0(r_1,r_2)P_{00}^{0S}(r_1,r_2,t)+V_{22,11}^0(r_1,r_2)P_{11}^{0S}(r_1,r_2,t), \quad (20)$$

where the operators V have the simple forms

$$V_{00,00}^0(r_1,r_2)=\frac{1}{r_>},$$

$$V_{00,11}^0(r_1,r_2)=-\sqrt{\frac{1}{3}}\frac{r_<}{r_>^2},$$

$$V_{00,22}^0(r_1,r_2)=\sqrt{\frac{1}{5}}\frac{r_<^2}{r_>^3},$$

$$V_{11,11}^0(r_1,r_2)=\frac{1}{r_>}+\frac{2}{5}\frac{r_<^2}{r_>^3},$$

$$V_{11,22}^0(r_1,r_2)=-\sqrt{\frac{4}{15}}\frac{r_<}{r_>^2}+\sqrt{\frac{27}{245}}\frac{r_<^3}{r_>^4},$$

$$V_{22,22}^0(r_1,r_2)=\frac{1}{r_>}+\frac{2}{7}\frac{r_<^2}{r_>^3}+\frac{2}{7}\frac{r_<^4}{r_>^5}. \quad (21)$$

Using the general forms found in Eqs. (5)–(7), the above coupled equations can be extended to include not only the s^2, p^2, and d^2 contributions, but higher ℓ^2 contributions.

The same 200×200 lattice used in Sec. III for the Temkin-Poet model was employed to solve Eq. (20). At time $t=0$ the initial radial wave function is given by Eq. (9) and shown in Fig. 1. We note that $P_{11}^{0S}(r_1,r_2,t=0)=P_{22}^{0S}(r_1,r_2,t=0)=0$. At time $t=25.0$ and 2500 time steps, the absolute value of a radial wave function with $S=0$ and $E=30$ eV is shown in Fig. 4, while the radial wave-function density with $S=1$ and $E=30$ eV is shown in Fig. 5. The frames in both figures are for the s^2, p^2, and d^2 radial wave functions.

Electron-impact ionization cross sections for $^{1,3}S$ scattering from hydrogen are presented in Tables III–V. In Table III convergence is demonstrated as a function of the number of close-coupled equations for the $^{1,3}S$ partial-wave cross sections at 30 eV incident energy. The rapid convergence in terms of $\ell_1\ell_2$ pairs is not unexpected. In first-order distorted-wave calculations for the ionization cross section, the number of ejected energy partial waves is generally small for all energies. Of course, in both the close-coupling and distorted-wave methods, the number of total LS partial waves increases with higher incident energies. In Tables IV and V the three-channel close-coupling calculations are compared with the time-independent converged close-coupling results of Bray and Stelbovics [9,35] at several incident energies.

The time-dependent close-coupling cross sections for the $^{1,3}S$ symmetries are compared with distorted-wave calculations in Figs. 6 and 7. The distorted-wave cross sections are

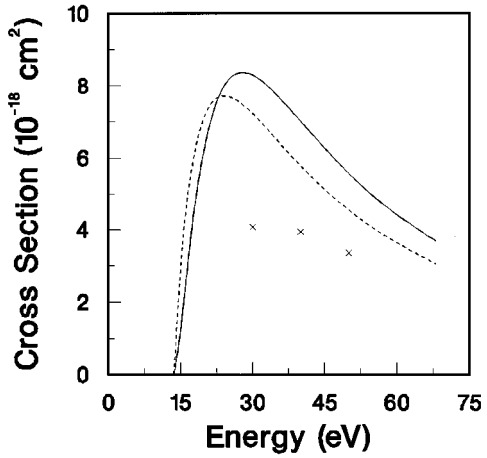

FIG. 10. Electron-impact ionization of hydrogen in the ^1P symmetry. Solid curve, distorted-wave method, prior form; dashed curve, distorted-wave method, post form; cross marks, time-dependent close-coupling method.

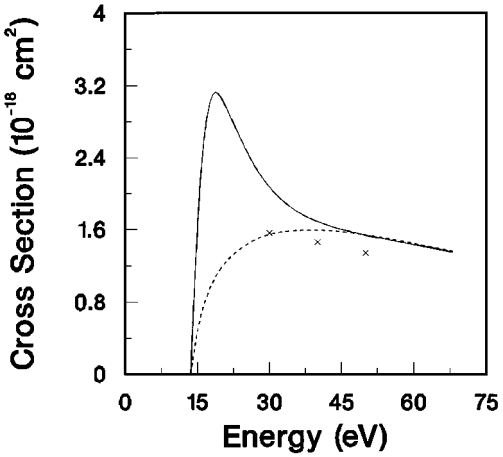

FIG. 11. Electron-impact ionization of hydrogen in the ^3P symmetry. Solid curve, distorted-wave method, prior form; dashed curve, distorted-wave method, post form; cross marks, time-dependent close-coupling method.

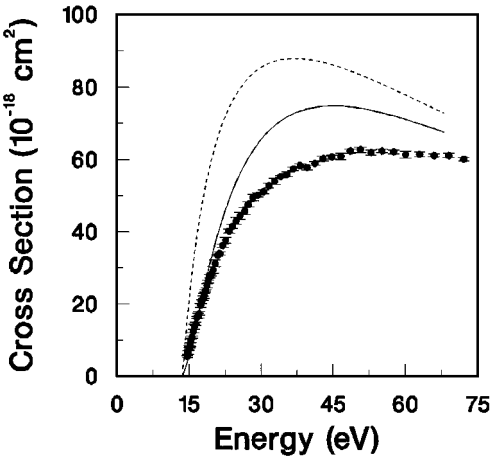

FIG. 12. Total electron-impact ionization cross section for hydrogen. Solid curve, distorted-wave method, prior form; dashed curve, distorted-wave method, post form; solid circles, experimental measurements [36].

based on a triple partial-wave expansion of the first-order scattering amplitude, including both direct and exchange terms. The prior form of the scattering amplitude [29] requires the incident and scattered electrons to be calculated in a V^N potential, while the bound and ejected electrons are calculated in a V^{N-1} potential. A post form of the scattering amplitude [30] may also be formulated in which all electrons are calculated in a V^{N-1} potential. For $L=0$ scattering, the post-form choice of distorted-wave method is in better agreement with the more exact close-coupling method.

V. $^{1,3}P$ PARTIAL-WAVE RESULTS

The same 200×200 lattice used for the $^{1,3}S$ partial-wave results was employed to solve Eqs. (5)–(7) for $L=1$. At time $t=0$ the initial radial wave function is given by Eq. (10) with $\ell=1$. At time $t=25.0$ and 2500 time steps, the absolute value of a radial wave function with $S=0$ and $E=30$ eV is shown in Fig. 8, while the radial wave-function density with $S=1$ and $E=30$ eV is shown in Fig. 9. Both are six-channel close-coupling calculations, including sp, ps, pd, dp, df, and fd contributions. The frames in both figures are for the sp, pd, and df radial wave functions. The ps, dp, and fd radial wave functions are the mirror images of the sp, pd, and df functions, respectively, the inversion axis being the $r_1=r_2$ line.

Electron-impact ionization cross sections for $^{1,3}P$ scattering from hydrogen are presented in Tables VI–VIII. In Table VI convergence is demonstrated as a function of the number of close-coupled equations for the partial wave cross sections at 30 eV incident energy. Again the convergence is found to be rapid in terms of $\ell_1\ell_2$ pairs. In Tables VII and VIII the six-channel close-coupling calculations are compared with the time-independent converged close-coupling results of Bray and Stelbovics [9,35] at several incident energies.

The time-dependent close-coupling cross sections for the $^{1,3}P$ symmetries are compared with distorted-wave calculations in Figs. 10 and 11. For $L=1$ scattering, the post-form choice of the distorted-wave method is in better agreement with the more exact close-coupling method. We caution against a choice for the best lowest-order distorted-wave method, however, since there remain large contributions to the total ionization cross section from higher partial waves. In fact, as shown in Fig. 12, the best agreement with the experimental measurements [36] of the total ionization cross section for hydrogen is found with the prior form of the distorted-wave method.

VI. SUMMARY

Based on the calculations presented in the previous sections, the time-dependent close-coupling method does quite well in describing the dynamics found in electron scattering from hydrogen. The method has its strength in a simple formulation and a freedom from matching to boundary conditions. The time evolution of the wave packet on the lattice provides a detailed picture of the short-time scattering dynamics. By projecting the wave packet onto stationary states of the target, a variety of inelastic scattering cross sections may be obtained. The ionization cross sections for various LS partial waves are in reasonable agreement with the current best theoretical results.

We regard the calculations presented here as preliminary in regard to numerical procedures. To better support one-electron bound states a variable mesh spacing could be employed. Half the lattice points could be eliminated by restricting the time propagation to the triangular region $r_1\leqslant r_2$. The Taylor-series propagator could be replaced by a more efficient method.

Finally, the time-dependent close-coupling calculations are essentially numerical experiments on simple systems. The types of systems could be extended through the use of core potentials and a single active electron approximation. It is important, however, to compare these numerical experiments with perturbation theory calculations to determine the dominant scattering mechanisms. Perturbation theory calculations still remain the only viable theoretical approach for many complex atoms and molecules.

ACKNOWLEDGMENTS

We would like to thank Dr. Igor Bray of Flinders University of South Australia, Dr. Wolfgang Ihra of the Technical University of Munich, and Dr. Don H. Madison of the University of Missouri at Rolla for several useful discussions. This work was supported in part by the National Science Foundation under Grant No. PHY-9122199 with Auburn University and the Office of Basic Energy Sciences, U.S. Department of Energy under Contract No. DE-AC05-84OR21400 with Lockheed-Martin Energy Systems, Inc. Computational work was carried out at the National Energy Research Supercomputer Center in Livermore, California.

[1] M. J. Seaton, Philos. Trans. R. Soc. London Ser. A **245**, 469 (1953).
[2] N. F. Mott and H. S. W. Massey, *The Theory of Atomic Collisions* (Oxford University Press, New York, 1971).
[3] *Atomic and Molecular Processes: An R-Matrix Approach*, edited by P. G. Burke and K. A. Berrington (IOP, London, 1993).
[4] J. Callaway and D. H. Oza, Phys. Rev. A **32**, 2628 (1985).
[5] I. E. McCarthy and Y. Zhou, Phys. Rev. A **49**, 4597 (1994).
[6] P. G. Burke, C. J. Noble, and M. P. Scott, Proc. R. Soc. London Ser. A **410**, 289 (1987).
[7] M. P. Scott and P. G. Burke, J. Phys. B **26**, L191 (1993).
[8] I. Bray and A. T. Stelbovics, Phys. Rev. Lett. **69**, 53 (1992).
[9] I. Bray and A. T. Stelbovics, Phys. Rev. Lett. **70**, 746 (1993).
[10] A. K. Bhatia, B. I. Schneider, and A. Temkin, Phys. Rev. Lett. **70**, 1936 (1993).
[11] D. A. Konovalov and I. E. McCarthy, J. Phys. B **27**, L407 (1994).
[12] F. Robicheaux, R. P. Wood, and C. H. Greene, Phys. Rev. A **49**, 1866 (1994).
[13] K. W. Meyer, C. H. Greene, and I. Bray, Phys. Rev. A **52**, 1334 (1995).
[14] A. Temkin, Phys. Rev. **126**, 130 (1962).
[15] J. Callaway and D. H. Oza, Phys. Rev. A **29**, 2416 (1984).
[16] M. LeDourneuf, J. M. Launay, and P. G. Burke, J. Phys. B **23**, L559 (1990).
[17] D. Kato and S. Watanabe, Phys. Rev. Lett. **74**, 2443 (1995).
[18] Y. D. Wang and J. Callaway, Phys. Rev. A **48**, 2058 (1993).
[19] Y. D. Wang and J. Callaway, Phys. Rev. A **50**, 2327 (1994).
[20] J. Botero and J. Shertzer, Phys. Rev. A **46**, R1155 (1992).
[21] J. Shertzer and J. Botero, Phys. Rev. A **49**, 3673 (1994).
[22] M. Brauner, J. S. Briggs, and H. Klar, J. Phys. B **22**, 2265 (1989).
[23] S. Jones, D. H. Madison, A. Franz, and P. L. Altick, Phys. Rev. A **48**, R22 (1993).
[24] E. O. Alt and A. M. Mukhamedzhanov, Phys. Rev. A **47**, 2004 (1993).
[25] C. Bottcher, Adv. At. Mol. Phys. **20**, 241 (1985).
[26] L. Zhang, J. M. Feagin, V. Engel, and A. Nakano, Phys. Rev. A **49**, 3457 (1994).
[27] D. R. Schultz, C. Bottcher, D. H. Madison, J. L. Peacher, G. Buffington, M. S. Pindzola, T. W. Gorczyca, P. Gavras, and D. C. Griffin, Phys. Rev. A **50**, 1348 (1994).
[28] W. Ihra, M. Draeger, G. Handke, and H. Friedrich, Phys. Rev. A **52**, 3752 (1995).
[29] S. M. Younger, Phys. Rev. A **22**, 111 (1980).
[30] J. H. Macek and J. Botero, Phys. Rev. A **45**, R8 (1992).
[31] R. Poet, J. Phys. B **11**, 3081 (1978).
[32] R. Poet, J. Phys. B **13**, 2995 (1980).
[33] R. Poet, J. Phys. B **14**, 91 (1981).
[34] I. Bray and A. T. Stelbovics, At. Data Nucl. Data Tables **58**, 67 (1994).
[35] I. Bray (private communication).
[36] M. B. Shah, D. S. Elliott, and H. B. Gilbody, J. Phys. B **20**, 3501 (1987).